Behavior of Post-Tensioned Concrete Girders Subject to Partially Strand Damage and Strengthened by NSM-CFRP Composites

Abbas Jalil [1*], Alaa Hussein Al-Zuhairi [1]

[1] Department of Civil Engineering, Faculty of Engineering, University of Baghdad, 10071 Baghdad, Iraq.

Abstract

Studies on the flexural behavior of post-tensioned beams subjected to strand damage and strengthened with near-surface mounted (NSM) technique using carbon fiber-reinforced polymer (CFRP) are limited and fail to examine the effect of CFRP laminates on strand strain and strengthening efficiency systematically. Furthermore, a design approach for UPC structures in existing design guidelines for FRP strengthening techniques is lacking. Hence, the behavior of post-tensioned beams strengthened with NSM-CFRP laminates after partial strand damage is investigated in this study. The testing program consists of seven post-tensioned beams strengthened by NSM-CFRP laminates with three partial strand damage ratios (14.3% symmetrical damage, 14.3% asymmetric damage, and 28.6% symmetrical damage). The experimental results showed that the use of CFRP laminates significantly increases the flexural capacity by up to 17.4 to 20.4%, corresponding to a strand damage ratio of 14.3 and 28.6%, respectively, enhances the stiffness, and reduces strand strain by up to 15.8 to 22.2%. However, the flexural stiffness of strengthened beams during serviceability phases is critical as strand damage ratios increase. Additionally, semi-empirical equations were proposed to predict the actual strain of unbonded strands whilst considering the effects of CFRP laminates. The suggested equations provide accurate predictions with little variance.

Keywords: NSM-CFRP Laminates; Post-Tensioned Concrete; Strand Damages; Strengthening.

1. Introduction

Post-tensioned concrete (PT) girders are widely used in bridges and large-span structures. Some of the strands and surrounding concrete may be damaged as a result of exposure to harsh weather conditions, high-vehicle collisions, etc. Consequently, partial loss of their structural capacity to resist stresses and an increase in deformation are expected. The process of replacing these members within sensitive facilities is often expensive and complicated. Therefore, the repair and strengthening of members are ideal options to ensure their return to the equivalent design capacity.

The Washington State Department of Transport (WSDOT) developed a set of criteria to describe damaged girder situations that would necessitate replacement without recourse to strengthening techniques. One of these criteria is that the strand damage rate exceeds 25%, and this requires researching the behavior of the members that have a higher strand damage rate using innovative strengthening methods [1]. Several field investigations have shown that CFRP materials may be applied to strengthen damaged PS bridge girders after severe concrete cross-section losses and a limited number of strand members have ruptured [2, 3].

External bonding (EB) and Near-Surface mounted (NSM) techniques are two common methods of strengthening and repairing concrete members using fiber-reinforced polymer (FRP) materials. The FRP material is characterized by

---

its ability to improve the structural performance of concrete members due to its high tensile strength, lightweight, and resistance to corrosion [4-7]. The fundamental concept behind these techniques is to apply FRP material to the tensile surface to enhance the flexural strength and stiffness of structural members. In the externally bonded technique, the CFRP sheets or laminates are bonded to the soffit of the concrete tensile surface using adhesive material, and this requires that the surface of the concrete cover be carefully prepared and leveled [8-10]. Whereas the use of the near-surface technique involves the inserting of CFRP rods or laminates along grooves made in the concrete cover that are bonded to the concrete surface using adhesives [11-13]. The SNM technique is more effective because the CFRP material is protected by the concrete cover, which provides more resistance to UV light and other weather issues, particularly with bridge girder strengthening. In addition, it is less susceptible to the risk of debonding due to the increase in the bonding area between the concrete and the CFRP material compared to that in the externally bonded (EB) technique [14, 15].

Although the FRP strengthening ACI 440-R guidelines cover most of the design approaches for concrete members, the design approach for strengthening the unbonded prestressed members has not been documented so far due to the scarcity of relevant research. This prompts designers to use design procedures for the bonded prestressed members, which often provide overestimated results [16, 17]. Predicting the flexural capacity of the bonded prestressing members is very simple because it depends on the strain compatibility principles of the critical section, which is different than that for the unbound prestressing members, which depends on the deformation for the entire length of the member [18].

The estimation of the strain increase of the strands represents a great challenge, which accordingly determines the flexural capacity of unbonded prestressed members. In the last decade, experimental studies were presented in conjunction with analytical studies to estimate the strain increase in the strand of the unbonded prestressed member with externally bonded techniques [16, 19]. Even though the success of these studies in formulating a design approach, these approaches were not included even in the latest version of the ACI 440-R, and this reflects the need to extend the research area to increase reliability in addition to investigating its validity with the NSM technique. The use of FRP strengthening significantly enhances the flexural capacity and reduces the rate of strand strain increase [16]. Reducing the strand strain is important because when some strands are damaged, this leads to a redistribution of the strains to the neighboring strands, which in turn may lead to an increase in the strains to a level that exceeds the permissible strains.

This study is a part of investigation research regarding the efficiency of strengthening techniques to enhance the flexural strength of unbonded post-tensioned concrete members that are conducted at Baghdad University-Civil Engineering Laboratories, and focuses on the Near-Surface Mounted strengthening techniques using CFRP laminate.

2. Materials and Methods

The research methodology is summarized in the flowchart shown in Figure 1.
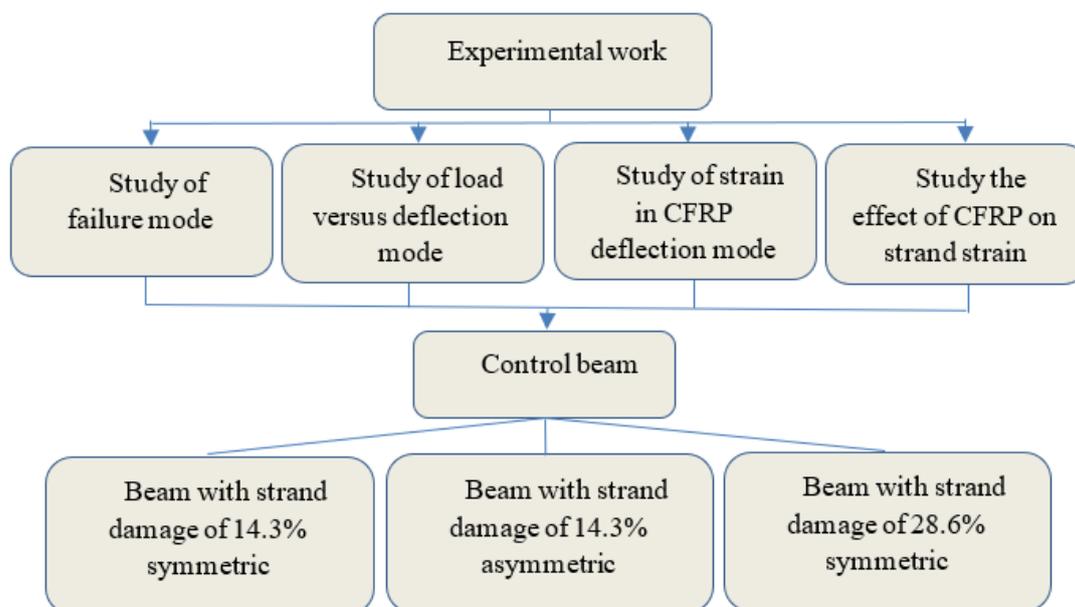
Figure 1. Flowchart for the research methodology

2.1. Materials and Beam Design

The experimental programme includes seven UPC simply supported beams with heights (h) of 300 mm, widths (b) of 200 mm, lengths (L) of 3000 mm, and an effective length (LO) of 2,800 mm. The concrete cover was 25 mm, except for tensile rebars, which use a concrete cover of 35 mm. The compressive strength, tensile strength, and modulus of

elasticity were obtained according to ASTM C39, ASTM C496-04, and ASTM C469, respectively (Table 1). The mixture proportions of the trial mix are presented in Table 2. The compressive and tensile strengths of the concrete estimated in 10 concrete cylinders (150 mm×300 mm) were 44.6 MPa and 5.1 MPa, respectively. The concrete had a slump of 118 ± 10 mm.

Table 1. Properties of the concrete

Compressive strength (f'_c) MPa	Tensile strength (f_{ct}) MPa	Modulus of elasticity (E_c) MPa
44.6	5.1	31,220

Table 2. The mixture proportions of the trial mix

Cement (kg/m³)	Coarse aggregates (kg/m³)	Coarse sands (kg/m³)	Fine sands (kg/m³)	Superplasticizer (Litter/m³)
415	1026	548	246	5.46

Three beams strengthened with CFRP laminates using the near-surface mounted technique were tested along with a control beam (REF) and three sub-reference beams (G1R, G2R, and G3R) with damaged strand ratios (DSR) of 14.3% (symmetric), 14.3% (asymmetric) and 28.6% (symmetric), the patterns of strand damage are illustrated in Figure 2.
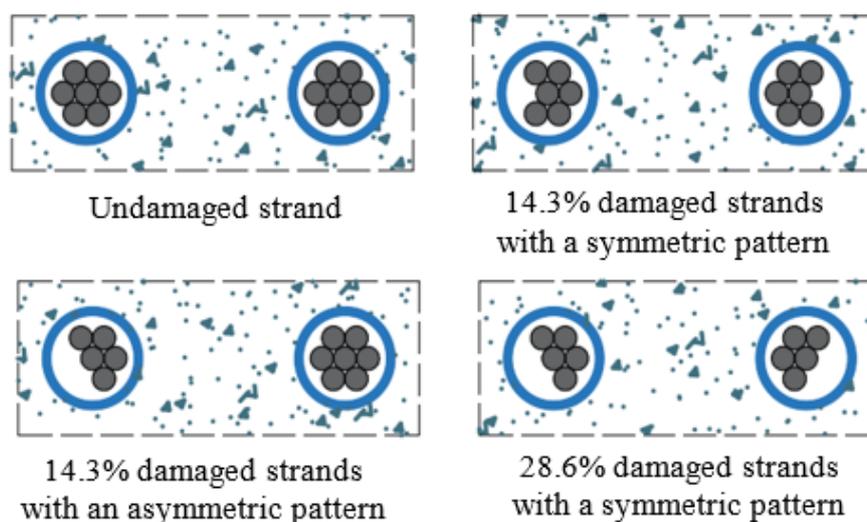
Figure 2. Patterns of damaged strands in the tested beams

Two types of steel reinforcement with diameters of 16 and 10 mm as shown in Table 3 were used for all beams in tension and compression zones, respectively. An appropriate amount of steel was used for shear reinforcement to avoid the occurrence of shear failure before flexural failure. Accordingly, closed stirrups with a diameter of 10 mm and a spacing of 100 mm c/c are placed along a length of 500 mm from the beam's edges and 200 mm c/c for the remaining middle length.

Table 3. Properties of the steel reinforcement

Type of steel	Diameter (mm)	Yield strength (MPa)	Ultimate Strength (MPa)	Maximum elongation (%)	modulus of elasticity (GPa)
rebar	10	518.2	658.97	12.2	200
rebar	16	577.3	710.74	13.4	200
strand	12.7	1725	1860	5	197.5

Two seven-wire low relaxations strands (12.7 mm) diameter and Grade (270) as presented in Table 3 were used for each UPC beam with a constant eccentricity of 70 mm extended inside PVC tubes as unbonded pre-stressing steel. Strand wires were carefully damaged as a result of the spiral form by fastening the two ends of the strand with metal cages and using an electric saw to achieve the specific ratio. Wedge-anchored prestressing strands were directly supported on a steel bearing plate (200 mm [width] × 80 mm [depth] × 12 mm [thickness]) attached to the ends of the beam. Two holes were formed on the steel plate to facilitate the application of prestressing. The steel plate was then installed on the formwork before pouring the concrete to ensure the centrality of strands and achieve complete contact with the concrete.

Three damaged beams were strengthened using a near-surface mounted technique utilizing two CFRP laminates with a cross-section of 1.2 mm width, 25 mm depth, and a length of 2000 mm (Table 4) The details of the tested beams are illustrated in Figures 3 and 4 and Table 5.

Table 4. Properties of CFRP laminates

Thickness (mm)	Fibre Density (g/cm³)	Tensile Modulus (GPa)	Tensile Strength (N/mm²)	Ultimate Elongation (%)
1.2	1.56	170	3,100	2
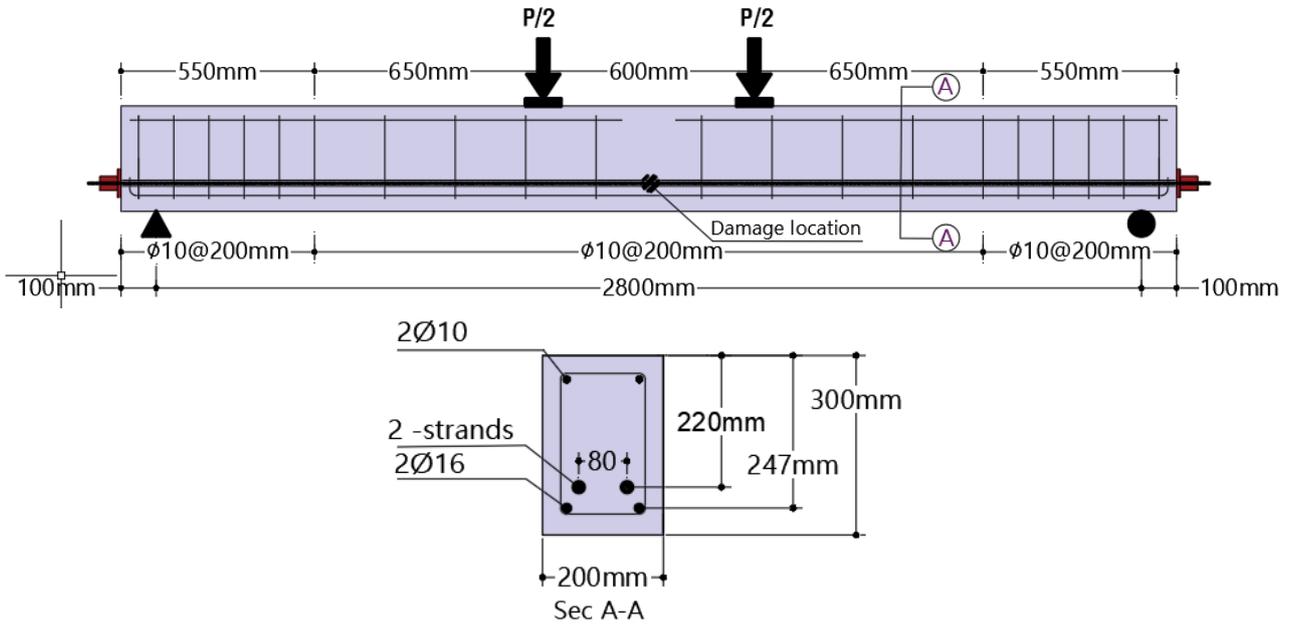
Figure 3. Details of the steel reinforcement for the tested
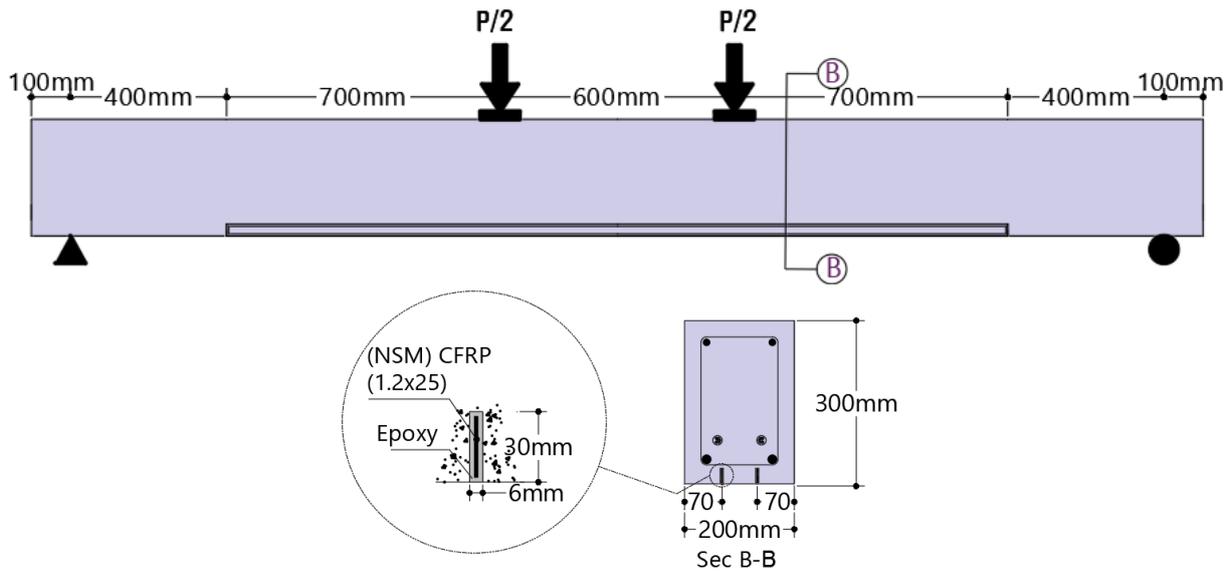
Figure 4. Details of CFRP-NSM-strengthened beams

Table 5. Summary of test parameters

Specimen	Strand damage ratio %	Damage pattern	A_{ps} (mm²)	ρ_p (%)	ρ_s (%)	CFRP laminate n× ($b_f × h_f$) (mm)
REF	0	---	197.4	0.49		---
G1R						---
G1N	14.3	Symmetric	169.2	0.385		2×1.4×25
G2R					0.81	---
G2N	14.3	Asymmetric	169.2	0.385		2×1.4×25
G3R						---
G3N	28.6	Symmetric	141	0.32		2×1.4×25

Note: n, b_f, and h_f- number, width, and height of CFRP laminates; W_f and H_f- width and height of sheet anchors.

Beams were post-tensioned by strands (according to specific damage ratios of each strand) with a straight trajectory after 28 days of casting and immediately before the strengthening process. The initial jacking stress in each strand was $0.6f_{pu}$ (Figure 5).

Figure 5. Post-tensioning process for the tested beams

CFRP laminates were installed one day after tensioning the beams and before installing the strengthening material, groove locations are first marked on the beams, which have been turned upside down. The concrete is cut to the required dimensions using a concrete saw. An air and water pressure jet is subsequently used to remove the remaining concrete particles in the grooves. CFRP laminates are then inserted after a layer of adhesive has been applied. The adhesive is leveled with the concrete surface using a scraper, as depicted in Figure 6. Each strengthened beam contained grooves with dimensions of 30 mm (depth) × 6 mm (width), as recommended by the ACI 440.2R-17 guideline [11].

Figure 6. Strengthening stages for the tested beams

2.2. Test Procedure and Instrumentation

The UPC beams were examined under two-point loading, as presented in Figure 7. The load is applied at a distance of 1100 mm from the closest support. The strain of the CFRP laminate was detected using strain gauges (resistance of 119.5±0.5 Ω), which were glued to the surface of the CFRP laminate at midlength. The tendon strain was measured using three strain gauges (119.5±0.5 Ω resistance) mounted at midlength, and loading locations. Notably, grooves were cut in the steel plate before installing anchors to prevent damaging the strain gauge wires. The strain of steel reinforcement was measured using one strain gauge (118.5±0.5Ω resistance) glued at the midlength, whilst two strain gauges (120±0.5Ω resistance, gauge length of 60 mm) were surface attached at compression and tension zones to monitor concrete strain. In addition, LVDTs were used to determine the girders' deflection. The data was automatically collected using a computerized data collecting system. To progressively raise the load, a hydraulic jack with a 500 kN capacity was used. A load cell with a 500 kN capacity was used to detect the load. On other hand, two dial gauges were used, one at the end of each strand, to check whether any strand slip occurred during the loading process.
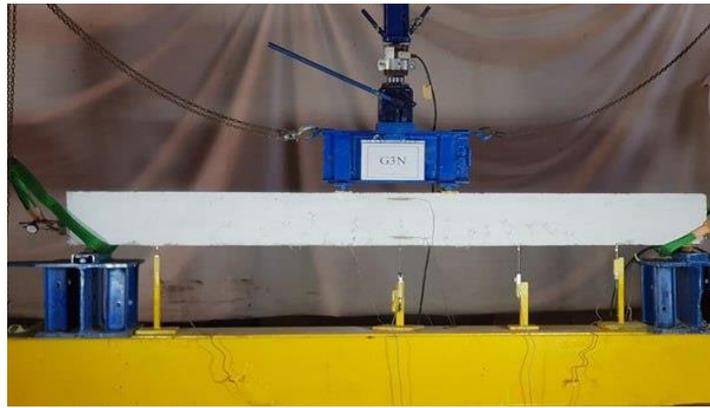
Figure 7. Test setup of experimental beams

3. Test Results and Discussion

3.1. Failure Mode

Flexural failure was observed in reference and sub-reference beams, with tensile steel reinforcing yielding, followed by concrete crushing in the compression zone, as shown in Figure 8. Compared with the strengthened beams, cracks develop faster, in fewer numbers, and with a wider crack width in the reference and sub-reference beams. The first flexural crack appears in the midspan of sub-reference beams G1R, G2R, and G3R, with cracking loads of the reference beam's cracking load at approximately 94.5%, 92%, and 85%, respectively. The cracking load reduces accompanied by an increase in the crack width when the ratio of strand damage increases.
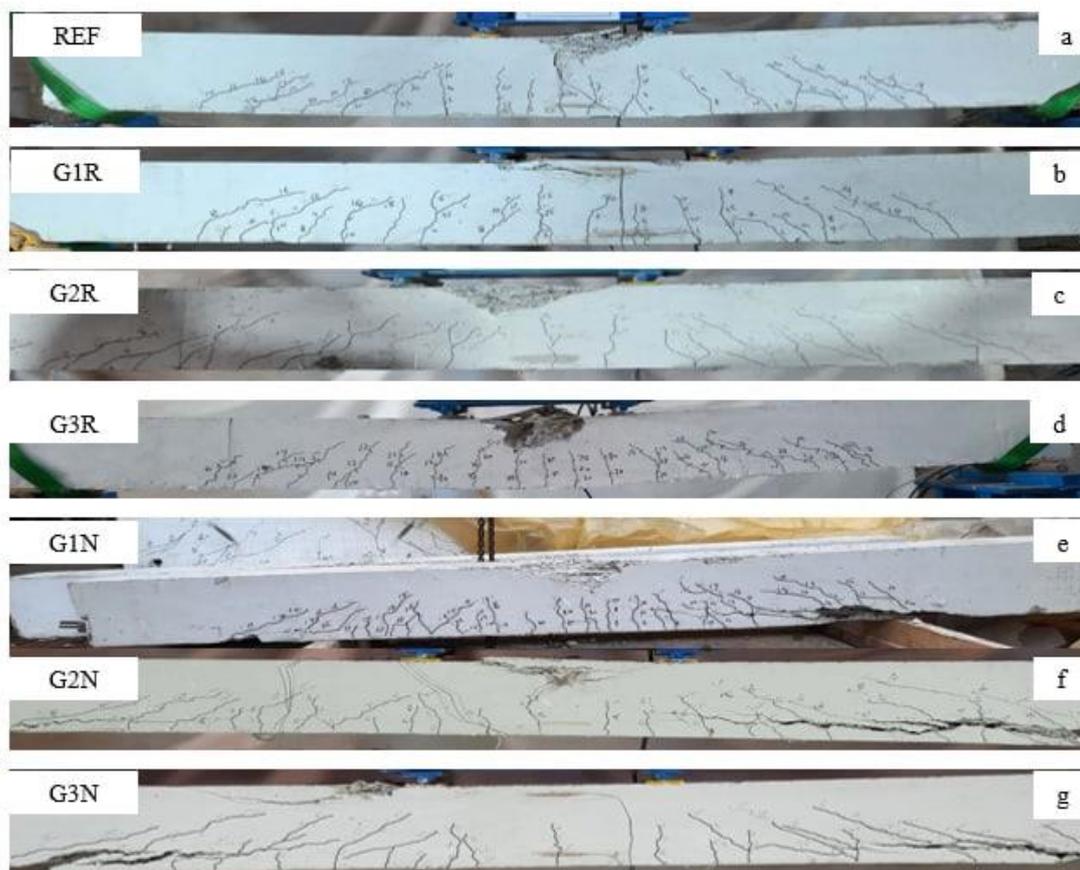
Figure 8. Failure pattern of the tested beams

The failure modes of the NSM-CFRP-strengthened beams were yielding of the tensile steel reinforcement and concrete cover separation after that (Figure 8). The failure of this type of strengthening showed higher brittleness, more cracks, and smaller crack widths than the corresponding sub-reference beams (Figure 9). The first flexural crack appears at the midspan of NSM-CFRP-strengthened beams G1N, G2N, and G3N, with an increase in the cracking load of 11%, 10%, and 13%, respectively, as compared with those of sub-reference beams.

Figure 9. Concrete cover separation and deboning of CFRP laminates

A crushing sound indicated the debonding of the CFRP laminate at approximately 85% of the ultimate load. However, the separation of the concrete cover occurred close to the end of CFRP laminates and developed rapidly along the shear span. According to an observation, concrete cover separation was caused by the significant increase of diagonal shear cracks that caused slip along longitudinal steel reinforcement and the concrete cover. Concrete cover separation or cover delamination and debonding of FRP from the concrete substrate are two failure modes associated with the use of FRP strengthening and discussed in detail in the ACI 440.2R-17 standard [17].

3.2. Load–Deflection Response

The flexural behavior of the investigated beams shown in Figure 10 was explored at three loading stages: elastic uncracked, allowable at the serviceability state, and ultimate loads.
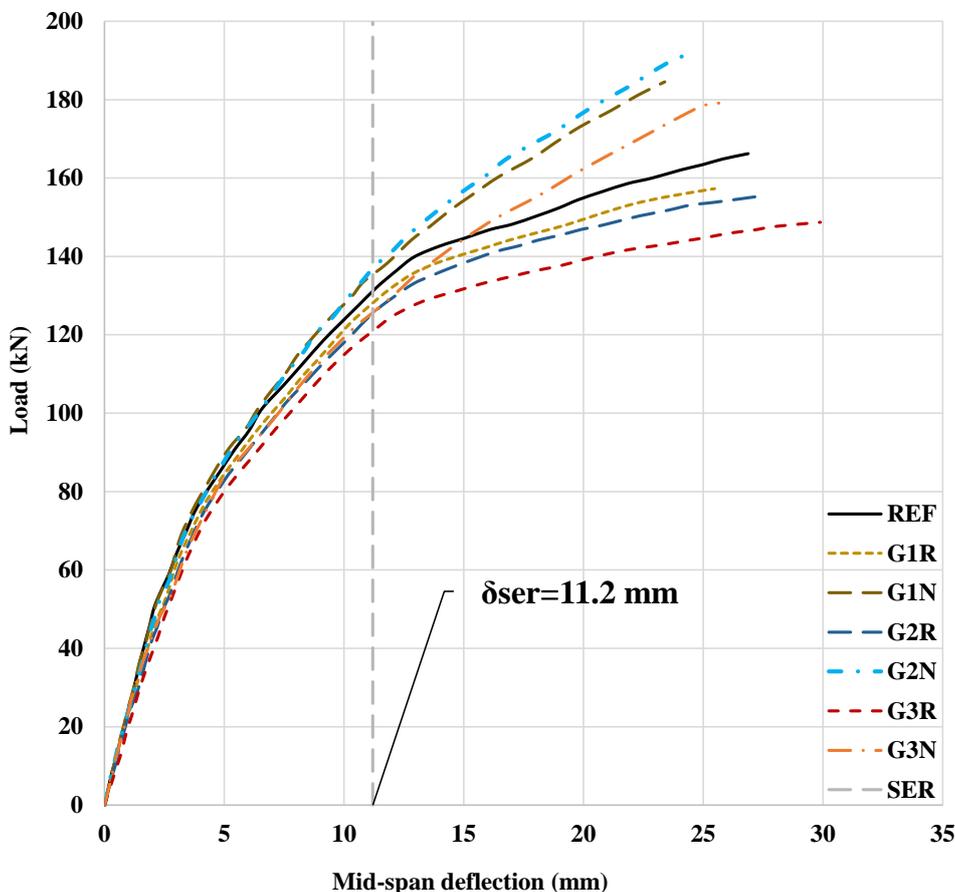
Figure 10. Load–deflection relationships at the midspan of the tested beams

The tested beams exhibited elastic linear behavior until the cracking load. The stiffness of reference beams slightly decreases as the ratio of damaged strands grows during this stage. The change in the stiffness of strengthened beams was non-significant compared with their counterparts from sub-reference beams. On other hand, sub-reference beams exhibit a rapid rate of stiffness degradation due to the loss of part of the prestressing force and an increase in the rate of crack development that increases deflection when applied loads exceed the crack load. Meanwhile, flexural-strengthening CFRP-NSM laminates demonstrated their effectiveness in delaying the development of cracks and postponing the stiffness degradation of strengthened beams. As a result, at the same load level, the strengthened specimens exhibited less deflection than the sub-reference specimens.

The applied load of the control beam was $P_{Ser,REF}= 0.79P_{u,REF}$ when it increased to a load level that produced a deflection corresponding to the permissible deflection ($Lo/250=11.2$ mm) at the serviceability state. This load is denoted by the allowable load at the serviceability state ($P_{Ser,REF}$).

The deflection of sub-reference beams G1R, G2R, and G3R (with an increase in the ratio of severed wires) increase by 6.2, 10.7, and 30.4%, respectively, compared with the control beam REF at the service load ($P_{Ser,REF}$). Whereas, the deflection of strengthened beams G1N, G2N, and G3N is reduced by 15.5, 19.2, and 31.3%, respectively, compared with that of their sub-reference counterparts.

The deflection of sub-reference beams generally increases compared with that of the control beam at all loading stages due to the reduction in prestressing forces that resist the effect of applied loads. Meanwhile, strengthened beams exhibit a reduction in deflection at the ultimate load due to the impeding of crack development during loading progress. The deflection for strengthened specimens G1N, G2N, and G3N was reduced by 9, 10, and 18%, respectively, compared with that of the corresponding sub-reference specimens.

The flexural strength of NSM-CFRP-strengthened beams G1N, G2N, and G3N was increased by 11, 15.5, and 7.7%, respectively, compared with that of the corresponding reference beam and by 17.4, 23.7, and 20.4% compared to sub-reference beams as presented in Table 6. By contrast, the flexural capacity of sub-reference beams G1R, G2R, and G3R had been reduced by 5.7, 7.1, and 11.8%, respectively, compared with that of the control beam REF.

Table 6. Test results

Beam	P_{cr} (kN)	P_u (kN)	$\delta_{u,mid}$ (mm)	M_u (kN.m)	Reduction in FS relative to REF (%)	Increase in FS relative to SUB-REF (%)	Failure mode
REF	55	166.24	26.9	91.43	---	---	SY-CC
G1R	52	157.25	25.5	86.49	5.7	---	SY-CC
G1N	58	184.56	23.4	101.51	---	11.0	SY-CCS-CC
G2R	5١	155.20	27.5	85.36	7.1	---	SY-CC
G2N	56	191.95	24.8	105.57	---	15.5	SY-CCS-CC
G3R	47	148.72	29.9	81.80	11.8	---	SY-CC
G3N	53	179.10	25.4	98.51	---	7.7	SY-CCS-CC

Note: FS-flexural strength, SY – bonded steel yielding, CC – concrete crushing, and CCS – concrete cover separation

Comparing the behavior of strengthened and REF beam is necessary because strengthened beams G1N and G2N (with a strand damage ratio of 14.3%) and the control beam REF behave similarly until the bonded rebar yields and results in a significant increase in displacement in the control specimen due to the rapidly increasing in crack width. Meanwhile, the strengthened beam G1N maintains a large portion of its stiffness even after yielding the bonded steel until concrete cover separation occurs. Moreover, as shown in Figure 10, the deflections in the strengthened beam G3N were higher than those detected in the reference beam at the same loading level until the load was approximately equal to 85% of the ultimate load of the reference beam. Even though the flexural capacity was restored for strengthened beams with strand damage of 28.6%, the service requirements (deflections versus loads along the service stages) should be verified for girders with strand damage of more than about 14.3%.

3.3. Strain in CFRP Laminates

The correlation between the increased load and the change in strain of CFRP laminates is presented in Figure 11. Before the cracking load, the strain of CFRP laminates in the strengthened beam is minimal and virtually equal. After the cracking load, the strain changes considerably, particularly after the yield of bonded steel reinforcement.

Load-Strain for FRP & Strand- G1
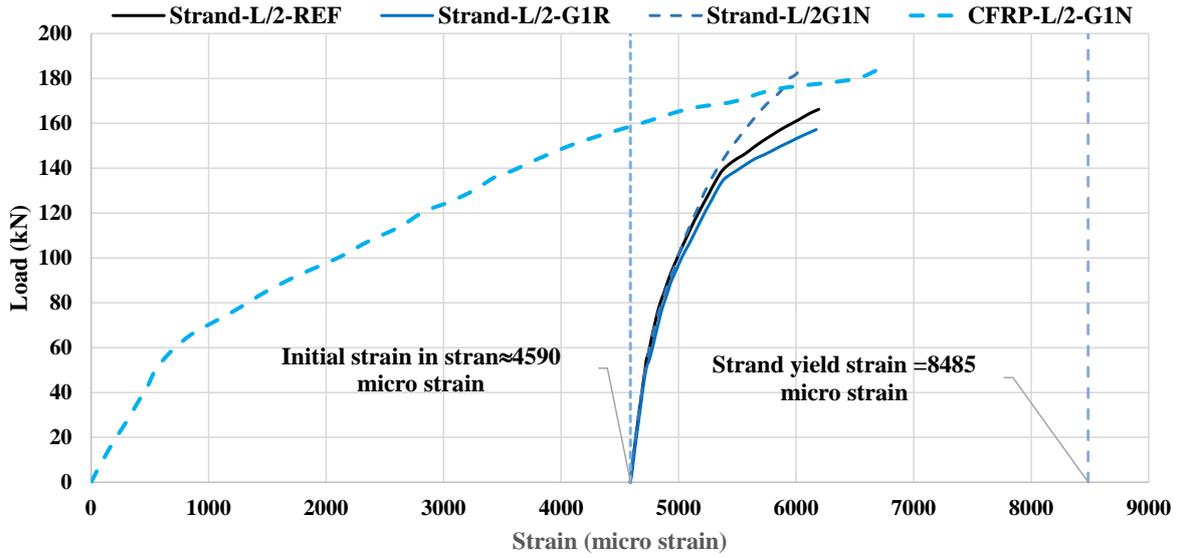
Load-Strain for FRP& Strand-G2

Load-Strain for FRP& Strand-G3

Load-Strain for FRP-G1, G2 & G3

Figure 11. Load-strain curves of tendons and CFRP laminates
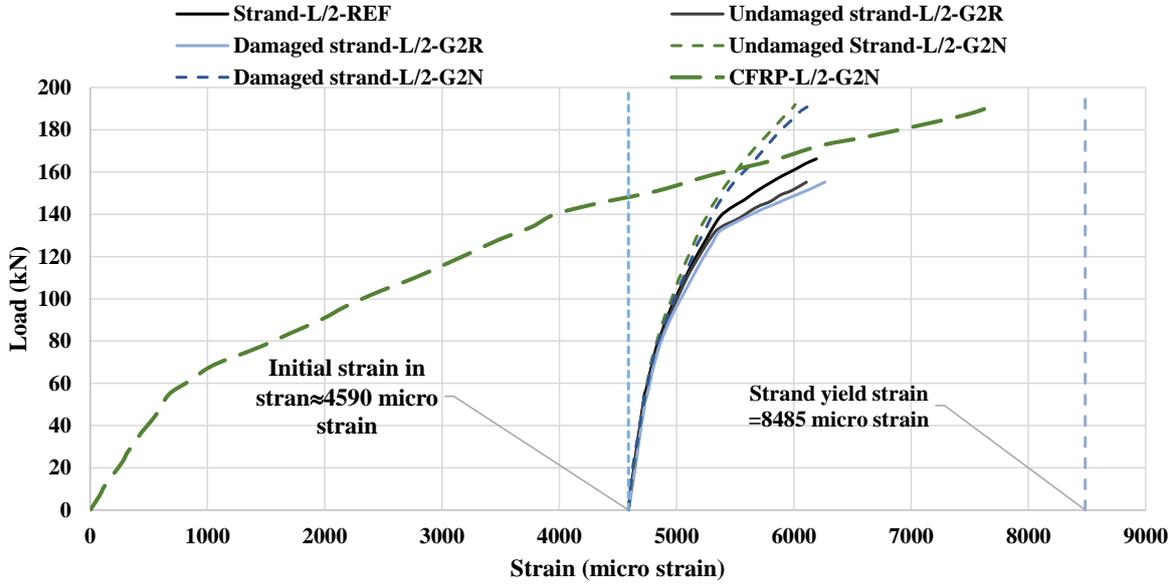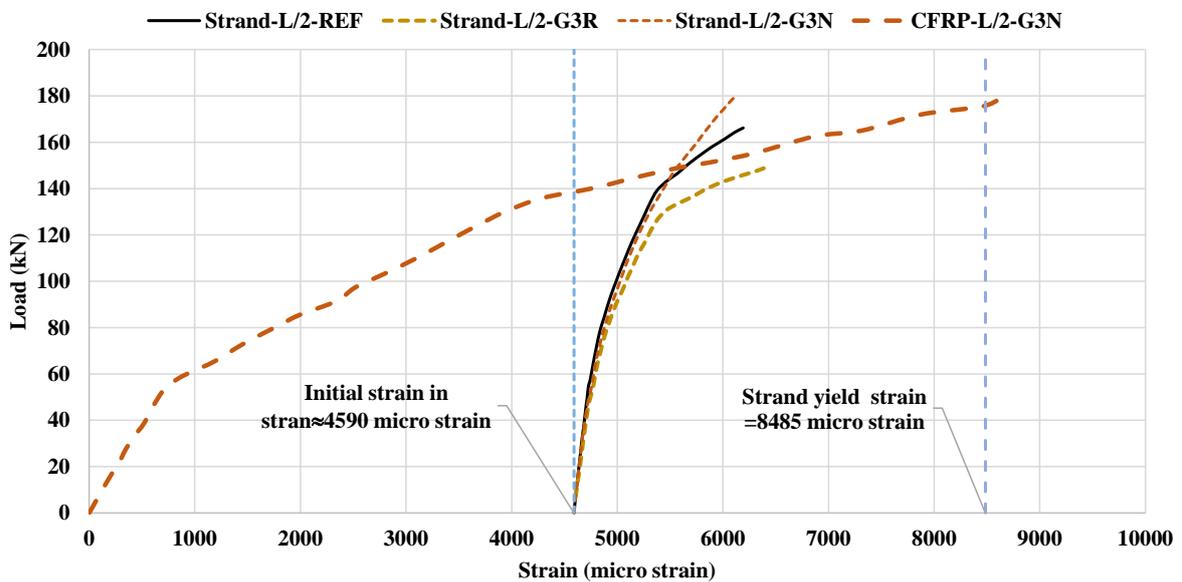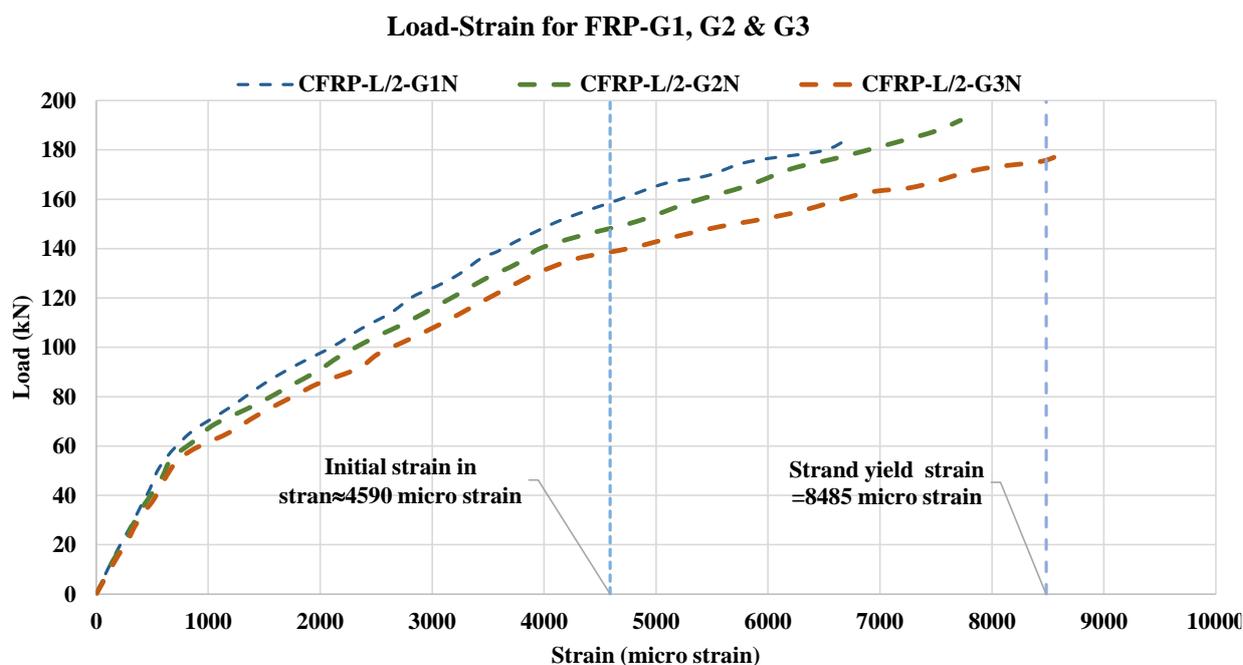
The increase in the strain at mid-length of CFRP laminates of strengthened beams G1N, G2N, and G3N was 0.34, 0.35, and 0.39%, respectively, which correspond to 17, 17.5, and 19.5% of the ultimate strain (ε_{ffu} =2%) at the service load. Meanwhile, the strain in the laminate at the ultimate loads was 0.66, 0.77, and 0.86%, corresponding to 33.4%, 38.5%, and 43% of the ultimate strain, respectively. According to these findings, the rate of strain rise in CFRP laminates increases as the damage in strands increases.

Furthermore, the application of CFRP laminates had a significant influence on the compressive strain of concrete. As indicated earlier, CFRP material effectively arrested cracks and delayed their development. This behavior led to a higher compressive concrete zone height for NSM-CFRP strengthened beams, resulting in reduced concrete strain in the strengthened specimens at the same loading level as sub-reference beams.

It is noted that the actual strains in the CFRP laminates did not exceed the maximum strain and that the failure modes are governed by the separation of the concrete cover along with the longitudinal rebar. This requires finding a mechanism to prevent the concrete cover separation, such as mechanical or U-wrapped sheet anchorages, which in turn exploits the rest of the available strains in the CFRP laminates, and therefore an increase in the flexural capacity and ductility is expected.

3.4. Strain in Strands and Influence of CFRP Laminates

The flexural strength is essentially unaffected by the change in prestressing force caused by a reduction in the cross-sectional area of the strands before the occurrence of the first crack due to a small increase in strand strain. As illustrated in Figure 11, the increase in strand strain was calculated by subtracting the initial effective strain (0.46%) from the actual strain. The behavior of strands was very similar amongst the investigated specimens during this stage. The strain of strands began to increase significantly after the cracking of beams. It can be observed that the increase in strand strain of sub-reference beams was higher than that indicated in the control beam. Whereas, at the same load level, the increase in strand strain of strengthened specimens was less than that of the sub-reference specimens.

The strain increase in the strands (which is considered as an average strain increase in two strands) at the permissible load of the control specimen ($P_{ser-REF}$) was about 0.0693%, whereas the corresponding increases in strand strains of sub-reference specimens G1R, G2R, and G3R were 0.0755, 0.0758, and 0.0894%; this finding showed an increase of 8.61, 9.71, and 29.6%, respectively, compared with those of the control specimen. Likewise, the strain increase in the strand of strengthened specimens G1N, G2N, and G3N was 0.0652, 0.0618, and 0.0732%, with a corresponding reduction of 15, 21, and 22%, respectively, compared with their counterparts in sub-reference specimens. The strengthened specimens G1N, G2N, and G3N exhibited a significant reduction in strand strain increase by 42.5, 73.1, and 25.6%, respectively, at the ultimate load of the control specimen.

The relationship is illustrated in Figure 11 clearly showed that the increase of strand strain in strengthened specimens G1N and G2N at the loading phase after the cracking load is smaller than that in control and sub-reference beams at the same load level; meanwhile, the strand strain of the strengthened beam G3N increased slightly in some parts of the

service load phases compared with that of the control beam REF and exhibited the same behavior as strengthened beams G1N and G2N compared with that of the sub-reference beam G2R. On other hand, by increasing the applied load and taking advantage of the strengthened beam's linear behavior, the strains in the strands (beam G3N) are reduced significantly, particularly after the yielding of steel reinforcement, as compared to the strain in the strands of the control beam.

Despite the considerable difference in strand strain increases for specimens G2R and G2N with asymmetric strand damage, the average strain increase in strands was close to that of strand specimens with symmetrical strand damage. At the allowable load, the coefficient of variation of strand strain increase for sub-reference specimens G1R and G2R was 0.09, while, it was 0.026 for strengthened beams G1N and G2N.

4. Computing Approach for FRP-strengthened Unbonded M_n Post-tensioned Members

Estimating the strain rise of the unbonded tendon is crucial in evaluating the flexural strength of UPC members strengthened with CFRP laminates. However, design approaches, such as ACI 440.2R-17, only include a guideline for estimating the change in the strain of bonded prestressing steel in PC girders strengthened with externally bonded FRP sheets whilst a corresponding procedure for prestressing steel in members strengthened with CFRP-NSM laminates is lacking. The experimental results showed that CFRP-NSM laminates significantly affect the behaviour of unbonded tendons.

The increase in strain and the flexural capacity of unbonded tendons are estimated in the present study using the procedure of El Meski and Harajli [19].

The following equations are suggested for evaluating the strain ε_{ps} in prestressing steel of CFRP Strengthened simply supported or continuous members at nominal flexural strength:

$$M_n = A_{ps}f_{ps}\left(d_p - \frac{\beta_1 c}{2}\right) + \Psi_f A_f E_f \varepsilon_f \left(d_f - \frac{\beta_1 c}{2}\right) + A_s f_s \left(d - \frac{\beta_1 c}{2}\right) \tag{1}$$

$$f_{ps} = F(\varepsilon_{ps}) \tag{1-a}$$

$$fs = E_s \varepsilon_s \leq f_y \tag{1-b}$$

$$\varepsilon_{ps} = N_p\, \varphi_{ps}\, \varepsilon_c \left(\frac{d_p - c}{L_a}\right) + \varepsilon_{pe} \tag{2}$$

where $\varepsilon_{pe} = f_{se} / E_{ps}$ (This formula represents the tendon's initial strain, not including stress losses), f_{se} which represents the effective stress of prestressing which is equal to F_p/A_p, N/mm², E_{ps} which represents the modulus of elasticity of the prestressing strand, (N/mm²), E_f represents the modulus of elasticity of the carbon fiber, N/mm², F_p which represents the tendon's initial tension force, (N), A_{ps} represents the tendon cross-sectional area, mm², A_f (mm²) represents the cross-sectional area of carbon fiber, mm², φ_{ps} which represents the stress reduction factor, set to 0.70, Ψ_f which represents the CFRP reduction factor, set to 0.85 as per, N_p (Unit less factor) which is represent the parameter considered for simply supporting members, Taking NP = 14.0 as a constant, [19].

Understanding that stress rarely of the prestressing reinforcement exceeds yield and limiting the related stress to $0.95f_{py}$ allows the use of a linear correlation between prestressing reinforcement strain and stress, i.e., $f_{ps} = E_{ps}.\varepsilon_{ps}$, which results as below:

$$f_{ps} = f_{se} + \left(\frac{\varphi_{ps}\, N_p\, E_{ps}\, \varepsilon_c}{L_a/d_p}\right)\left(1 - \frac{c}{d_p}\right) \leq 0.95f_{py} \tag{3}$$

The equilibrium tension and compression forces across the rectangular section can be stated as follows, assuming rectangular section actions:

$$Aps\, f_{ps} + A_f E_f \varepsilon_f + A_s f_s = \alpha_1 f_c' b \beta_1 c \tag{4}$$

$$\varepsilon f = \varepsilon_{cu}\left(\frac{d_f - c}{c}\right) - \varepsilon_{bi} \leq \varepsilon_{fd} \tag{5}$$

$$\varepsilon_{fd} = 0.7\varepsilon_{fu} \tag{6}$$

$$\varepsilon_{fd} = 0.41\sqrt{\frac{f'c}{n_f E_f t_f}} \cdot \leq 0.9\varepsilon_{fu} \tag{7}$$

where ε_{fd} which represents the debonding strain of the carbon fiber, microstrain.

The following step-by-step approach may be used to determine the nominal moment capacity M_n of NSM-CFRP strengthened unbonded post-tensioned members using Equations 2 to 4. According to ACI 440.2R-17, use Equation 6 instead of Equation 7 which is acceptable for the externally bonded technique [20].

Form I: Concrete crushing governs flexural strength.

1st Step: Assume that concrete crushing governs the nominal capacity, ε_f Equation 5 is less than or equal to ε_{fd} Equation 7-a. This implies that $\varepsilon_c = \varepsilon_{cu}$, $\alpha_1 = 0.85$ and β_1 is as described in section 10.2.7.3 of the ACI-318 [21]. Replacing f_{ps} from Equation 3 into Equation 4 and assuming that the bonded steel yields [22], i.e., $f_s = f_y$, This provides in the quadratic equation follows, which is then used to determine the NA depth at nominal capacity in the critical section:

$$c = \frac{B+\sqrt{B^2+4.A.C}}{2.A} \tag{8}$$

$$A = 0.85.\beta_1.f_c'.b + \frac{\varphi_{ps}.N_p.A_{PS}.\varepsilon_{cu}}{L_a}.A_{PS} \tag{8-a}$$

$$B = A_{ps}\left(f_{se} + \frac{\varphi_{ps}.N_pE_{ps}.\varepsilon_{cu}.d_p}{L_a}\right) - A_f.E_f.(\varepsilon_{cu} + \varepsilon_{bi}) + A_s.f_y \tag{8-b}$$

$$C = A_f.E_f.\varepsilon_{cu}.d_f \tag{8-c}$$

2nd Step: If ε_f Equation 5 less than ε_{fd}. Inspect if the strain in the bonded rebar ε_s is higher than the strain at yield ε_y. If $\varepsilon_f \leq \varepsilon_{fd}$ whereas ε_s is lower than ε_y, regenerate the 1st step to recompute the NA depth more precisely using Equation 9 when substituting, the following set of quadratic parameters is generated $f_s = E_s (\varepsilon_s = \varepsilon_{cu}(d-c)/c)$ instead of $f_s = f_y$ in Equation 4:

$$c = \frac{B + \sqrt{B^2 + 4.A.C}}{2.A} \tag{9}$$

$$A = 0.85.\beta_1.f_c'.b + \frac{\varphi_{ps}.N_p.A_{PS}.E_{ps}.\varepsilon_{cu}}{L_a}.A_{PS} \tag{9-a}$$

$$B = \left(\frac{\varphi_{ps}.N_p.E_{ps}.\varepsilon_{cu}.d_p}{L_a} + f_{se}\right).A_{ps} - A_s.E_s.\varepsilon_{cu} - A_f.E_f.(\varepsilon_{cu} + \varepsilon_{bi}) \tag{9-b}$$

$$C = A_f.E_f.\varepsilon_{cu}.d_f + A_s.E_s.\varepsilon_{cu}.d \tag{9-c}$$

3nd Step: Calculate f_{ps} from Equation 3 as per $\varepsilon_c = \varepsilon_{cu}$, and $f_s = E_s\varepsilon_s \leq f_y$, and compute M_n from Equation 1

Form II: FRP Failure governs flexural strength

4th Step: If ε_f computed as per Equation 5 is higher than the debonding strain (ε_{fd}) in Equation 6, then FRP failure occurs before the strain ε_c in the most distant concrete compression fiber reaches ε_{cu}. In this case, the strain ε_f in the FRP laminates are equal to ε_{fd}, As a result, a trial-and-error technique for ensuring strain compatibility and forces equilibrium over the depth of the critical section becomes more appropriate, as described in the following steps.

5th Step: Adopting the value of $\varepsilon_f = \varepsilon_{fd}$ in addition to an assumed initial value of neutral axis depth (*c*), determine the strain in concrete ε_c at the extreme concrete compression fiber from Equation 10, and compute the stress in the unbonded prestressing steel using Equation 3 and the stress in the bonded reinforcing steel from Equation 11 replacing ε_{cu} by ε_c.

$$\varepsilon_c = \varepsilon_{fd}.\frac{c}{d_f-c} \tag{10}$$

$$f_s = E_s.\varepsilon_c.\frac{d-c}{c} \tag{11}$$

6th Step: review the equilibrium condition using Equation 4 in which $\varepsilon_f = \varepsilon_{fd}$, and α_1 and β_1 are computed as pr Equations 12 and 13, respectively:

$$\beta_1 = \frac{4\varepsilon_c' - \varepsilon_c}{6\varepsilon_c' - 2\varepsilon_c} \tag{12}$$

$$\alpha_1 = \frac{3\varepsilon_c\varepsilon_c' - (\varepsilon_c)^2}{3\beta_1(\varepsilon_c')^2} \tag{13}$$

in which ε_c' is the strain corresponding to the ultimate compressive stress in concrete f_c', which can be considered equal to 0.0021 or computed as $\varepsilon_c' = 1.7\frac{f_c'}{E_c}$.

7th Step: Steps 5, and 6 need to be repeated by modifying the depth c until the force equilibrium condition are met in Equation 4 are approximately equal.

8th Step: Using Equation 1, determine the value of the nominal flexural strength M_n at the critical section, where $\varepsilon_f = \varepsilon_{fd}$.

9th Step: Check if $\varphi M_n \geq M_u$, where M_u is the externally applied moment.

As the result, the experimental values of ultimate stress gained unbonded strands were compared to those predicted by the previously given equations [11]. As indicated in Figure 12 and Table 7, the COV for theoretical and practical moments was 0.0870.
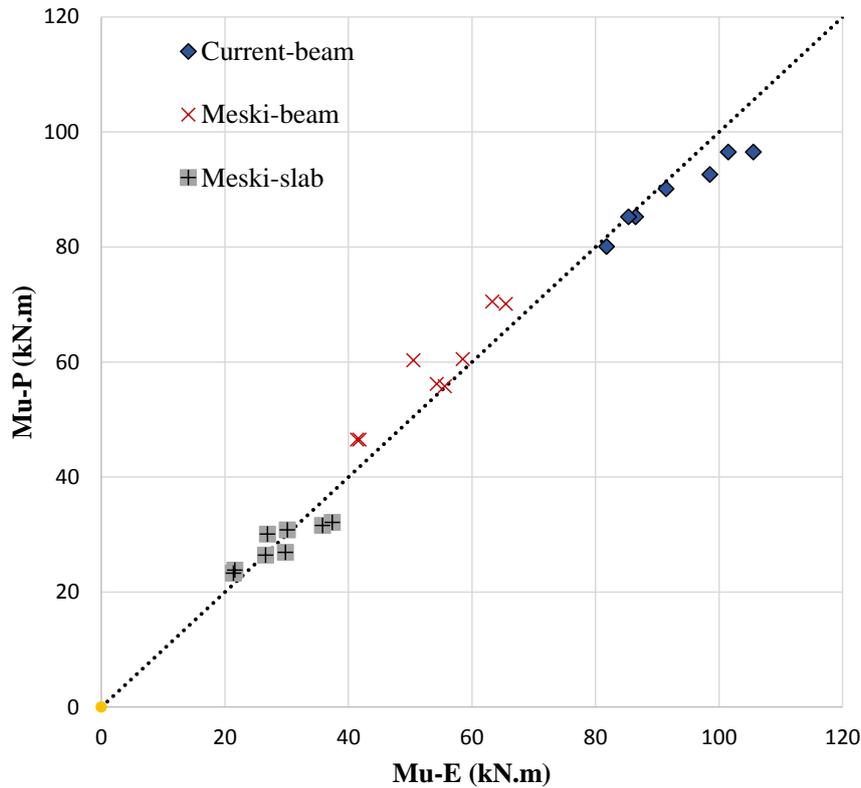
Figure 12. Experimental vs. predicted values of flexural capacities

Table 7. Predicted and experimental flexural capacities

Members for (El Meski & Harajli, 2013) [19]				Current study results			
Specimens	M_{u-P}	M_{u-E}	M_{u-E}/M_{u-p}	Specimens	M_{u-p}	M_{u-E}	M_{u-E}/M_{u-p}
UB1_H_F1	41.8	46.5	0.90	REF	91.43	90.11	1.01
UB1_H_F2	54.3	56.2	0.97	G1R	86.49	85.24	1.01
UB1_P_F1	41.4	46.5	0.89	G1N	101.51	96.51	1.05
UB1_P_F2	55.6	55.8	1.00	G2R	85.36	85.24	1.00
UB2_H_F1	50.5	60.3	0.84	G2N	105.57	96.51	1.09
UB2_H_F2	65.5	70.1	0.93	G3R	81.8	80.07	1.02
UB2_P_F1	58.5	60.5	0.97	G3N	98.51	92.59	1.06
UB2_P_F2	63.3	70.5	0.90	Average			1.04
US1-H-F1	21.4	23.3	0.92	Standard of deviation			0.03
US1_H_F2	26.9	30.1	0.89	COV			0.032
US1_P_F1	21.6	23.8	0.91				
US1_P_F2	30.1	30.8	0.97				
US2_H_F1	26.6	26.4	1.01				
US2_H_F2	35.8	31.6	1.13				
US2_P_F1	29.8	26.9	1.11				
US2_P_F2	37.4	32.1	1.16	**For all members**			
Average			0.97	Mean			0.990
Standard of deviation			0.09	Standard of deviation			0.086
Coefficient of variation COV			0.097	COV			0.0870

M_{u-E} and M_{u-P} is experimental and predicted flexural moment capacity

5. Conclusions

The behavior of unbonded post-tensioned concrete girders subjected to partial strand damage and strengthened by NSM-CFRP laminates was investigated in this paper. The following conclusions may be taken from this study's experimental results.

- The flexural capacity of post-tensioned beams reduces as the strand damage ratio increases, whilst the deflection of beams increases as the ratio of strand damage increases at the same loading level. The flexural capacity was reduced by 6% and 12% for beams with symmetrical strand damage of 14.3 and 28.6%, respectively. Meanwhile, the flexural capacity of beams with asymmetric strand damage of 14.3% was reduced by 7%.

- Near-surface mounted techniques using CFRP laminates enhance the cracking load and flexural capacity by controlling the crack development. The NSM-CFRP laminates increase both the cracking load and the flexural strength of damaged UPC beams to a maximum of 23.6 and 11.5%, respectively.

- The behavior of strands is considerably influenced by CFRP laminates. At the same loading level, the strain increase of strands in strengthened beams was much less than that of damaged beams. At the service load of the undamaged control beam, for instance, the increase in strand strain of the strengthened beams is decreased by 15 to 22% compared to the corresponding damaged beams.

- Concrete cover separation is a prevalent failure mode of NSM-strengthened members, which in turn reduces the flexural strength capacity. This requires broadening the research area to include testing of mechanical and U-wraped sheet anchors, which prevent concrete separation and are likely to increase flexural strength and enhance ductility.

- Even with the restoration of the flexural capacity of the strengthened members with a strand damage of more than 14.3%, the deflections along the service stages of the strengthened members are higher than those of the undamaged members, which may be critical for some sensitive structural projects.

- The suggested approach for estimating strand strain increases in unbonded post-tension members enhanced with NSM-CFRP laminates predicts flexural strength with variance (Mean = 0.99 and COV = 0.0870).

6. Declarations

6.1. Author Contributions

A.J.D. and A.H.A. contributed to the design and implementation of the research, to the analysis of the results and to the writing of the manuscript. All authors have read and agreed to the published version of the manuscript.

6.2. Data Availability Statement

The data that support the findings of this study are available on request from the corresponding author.

6.3. Funding

The authors received no financial support for the research, authorship, and/or publication of this article.

6.4. Conflicts of Interest

The authors declare no conflict of interest.

7. References

[1] Brice, R. (2013). Precast-Prestressed Concrete Girders Damaged by Over-Height Load Impacts. Washington State Department of Transportation, Olympia, United States.

[2] ElSafty, A., Graeff, M. K., & Fallaha, S. (2014). Behavior of Laterally Damaged Prestressed Concrete Bridge Girders Repaired with CFRP Laminates Under Static and Fatigue Loading. International Journal of Concrete Structures and Materials, 8(1), 43–59. doi:10.1007/s40069-013-0053-0.

[3] Di Ludovico, M., Prota, A., Manfredi, G., & Cosenza, E. (2010). FRP Strengthening of Full-Scale PC Girders. Journal of Composites for Construction, 14(5), 510–520. doi:10.1061/(asce)cc.1943-5614.0000112.

[4] Syahrul, S., Tjaronge, M. W., Djamaluddin, R., & Amiruddin, A. A. (2021). Flexural Behavior of Normal and Lightweight Concrete Composite Beams. Civil Engineering Journal, 7(3), 549–559. doi:10.28991/cej-2021-03091673.

[5] Kalfat, R., Gadd, J., Al-Mahaidi, R., & Smith, S. T. (2017). Evaluation and classification of anchorage systems used to enhance the flexural performance of FRP strengthened concrete members. SP-327: The 13th International Symposium on Fiber-Reinforced Polymer Reinforcement for Concrete Structures. doi:10.14359/51713356.

[6] Slaitas, J., & Valivonis, J. (2021). Full moment-deflection response and bond stiffness reduction of RC elements strengthened with prestressed FRP materials. Composite Structures, 260, 113265. doi:10.1016/j.compstruct.2020.113265.

[7] Siddika, A., Mamun, M. A. Al, Alyousef, R., & Amran, Y. H. M. (2019). Strengthening of reinforced concrete beams by using fiber-reinforced polymer composites: A review. Journal of Building Engineering, 25, 100798. doi:10.1016/j.jobe.2019.100798.

[8] Balamuralikrishnan, R., & Saravanan, J. (2021). Effect of addition of alccofine on the compressive strength of cement mortar cubes. Emerging Science Journal, 5(2), 155-170. doi:10.28991/esj-2021-01265.

[9] Hosen, M. A., Jumaat, M. Z., Alengaram, U. J., Sulong, N. H. R., & Islam, A. B. M. S. (2019). Structural performance of lightweight concrete beams strengthened with side-externally bonded reinforcement (S-EBR) technique using CFRP fabrics. Composites Part B: Engineering, 176, 107323. doi:10.1016/j.compositesb.2019.107323.

[10] Singh, V., & Sangle, K. (2022). Analysis of Vertically Oriented Coupled Shear Wall Interconnected with Coupling Beams. HighTech and Innovation Journal, 3(2), 230–242. doi:10.28991/hij-2022-03-02-010.

[11] Al-Saadi, N. T. K., Mohammed, A., Al-Mahaidi, R., & Sanjayan, J. (2019). A state-of-the-art review: Near-surface mounted FRP composites for reinforced concrete structures. Construction and Building Materials, 209, 748–769. doi:10.1016/j.conbuildmat.2019.03.121.

[12] Panahi, M., Zareei, S. A., & Izadi, A. (2021). Flexural strengthening of reinforced concrete beams through externally bonded FRP sheets and near surface mounted FRP bars. Case Studies in Construction Materials, 15, 601. doi:10.1016/j.cscm.2021.e00601.

[13] Nurbaiah, M. N., Hanizah, A. H., Nursafarina, A., & Nur Ashikin, M. (2010). Flexural behaviour of RC beams strengthened with externally bonded (EB) FRP sheets or Near Surface Mounted (NSM) FRP rods method. 2010 International Conference on Science and Social Research (CSSR 2010). doi:10.1109/CSSR.2010.5773725.

[14] Abdallah, M., Al Mahmoud, F., Boissière, R., Khelil, A., & Mercier, J. (2020). Experimental study on strengthening of RC beams with Side Near Surface Mounted technique-CFRP bars. Composite Structures, 234, 111716. doi:10.1016/j.compstruct.2019.111716.

[15] Jones, M. S. (2017). Repair of Impact-Damaged Prestressed Bridge Girders Using Strand Splices and Fabric Reinforced Cementitious Matrix. Master Thesis, Virginia tech, Blacksburg, United States.

[16] Nguyen-Minh, L., Phan-Vu, P., Tran-Thanh, D., Phuong Thi Truong, Q., Pham, T. M., Ngo-Huu, C., & Rovňák, M. (2018). Flexural-strengthening efficiency of cfrp sheets for unbonded post-tensioned concrete T-beams. Engineering Structures, 166, 1–15. doi:10.1016/j.engstruct.2018.03.065.

[17] ACI 440.2R-17. (2017). Guide for the Design and Construction of Externally Bonded FRP Systems for Strengthening Concrete Structures. American Concrete Institute, Farmington Hills, United States. doi:10.14359/51700867.

[18] Peera, I., & Oukaili, N. (2021). Experimental Study on the Behaviours of Post-tensioned Concrete Members with Unbonded Tendons. IOP Conference Series: Materials Science and Engineering, 1067(1), 012033. doi:10.1088/1757-899x/1067/1/012033.

[19] El Meski, F. M., & Harajli, M. H. (2013). Flexural Capacity of FRP Strengthened Unbonded Prestressed Concrete Members: Proposed Design Guidelines. 11th International Symposium on Fiber Reinforced Polymers for Reinforced Concrete Structures, FRPCS-11, 26-28 June 2013, Portugal.

[20] Abbas, H. Q., & Al‑Zuhairi, A. H. (2022). Usage of EB-CFRP for Improved Flexural Capacity of Unbonded Post-Tensioned Concrete Members Exposed to Partially Damaged Strands. Civil Engineering Journal, 8(6), 1288‑1303. doi:10.28991/cej-2022-08-06-014.

[21] ACI 318-19. (2019). Building code requirement for reinforced concrete (ACI 318-19)-Commentary on building Code Requirements for Structural Concrete (ACI 318R-19). American Concrete Institute, Farmington Hills, United States.

[22] Al-Zuhairi, A. H., Al-Ahmed, A. H., Abdulhameed, A. A., & Hanoon, A. N. (2022). Calibration of a New Concrete Damage Plasticity Theoretical Model Based on Experimental Parameters. Civil Engineering Journal, 8(2), 225–237. doi:10.28991/cej-2022-08-02-03.